Key Engineering Materials
ISSN: 1662-9795, Vol. 1024, pp 67-72
doi:10.4028/p-qsEbu9

Submitted: 2024-09-20
Revised: 2025-08-01
Accepted: 2025-08-04
Online: 2025-09-12

SiC Avalanche Photodiodes - Crystal Orientation and Spatial Uniformity

Daniel Habersat[1,a*], Anand Sampath[1,b], Greg Garrett[1,c], Michael Derenge[1,d], Franklin Nouketcha[1,e], Brenda VanMil[1,f], Michael Wraback[1,g], Jonathan Schuster[1,h], Jeremy Smith[1,i], Enrico Bellotti[2,j], Mike Zhu[2,k], Reza Ghandi[3,l], and Mehrnegar Aghayan[3,m]

[1]DEVCOM Army Research Laboratory, 2800 Powder Mill Road, Adelphi, MD 20783 USA

[2]Boston University, Department of ECE, 8 St. Mary's Street, Boston, MA 02215, USA

[3]GE Aerospace Research, 1 Research Circle, Niskayuna, NY 12309, USA

[a]daniel.b.habersat.civ@army.mil, [b]anand.v.sampath.civ@army.mil, [c]gregory.a.garrett.civ@army.mil, [d]michael.a.derenge.civ@army.mil, [e]franklin.l.nouketcha.civ@army.mil, [f]brenda.l.vanmil.civ@army.mil, [g]michael.wraback.civ@army.mil, [h]jonathan.schuster2.civ@army.mil, [i]jeremy.l.smith135.ctr@army.mil, [j]bellotti@bu.edu, [k]mjzhu@bu.edu, [l]ghandi@ge.com, [m]Mehrnegar.Aghayan@ge.com

Keywords: avalanche, photodiode, spatial uniformity, single photon, UV detector

Abstract. We are investigating 4H-SiC avalanche photodiodes for use as solar-blind, single-photon UV detectors, which could enable low cost, size, weight, and power devices that are reliable and robust, suitable for many sensing applications. One concern for these devices is the spatially-nonuniform gain which limits the useful device area and impedes the scaling necessary to compete with leading UV sensor architectures. We examined various potential sources of the nonuniformity, and conclude that the typically observed phenomenon is likely caused by impact ionization anisotropy and the 4° wafer offcut angle needed to maintain a consistent polytype during epitaxial growth. Additionally, we present both linear and Geiger-mode spatial maps on the same devices to explain the observed differences in each.

Introduction

SiC is attractive for UV single-photon avalanche detectors (SPADs) as it is inherently blind to visible light, and photon counting (i.e., Geiger mode) as well as high-gain linear-mode devices have been demonstrated [1, 2]. However, issues remain regarding bias-dependent spatial uniformity of detection efficiency (DE) and responsivity [3, 4, 5]. Specifically, Guo et al. [3] observed increasing spatial non-uniformity with gain in 4H SiC APDs in linear-mode operation for gain below 10,000. In contrast, Cai et al. [4] observed that the Geiger-mode spatial nonuniformity of SiC avalanche photodiodes (APDs) was poor at low excess bias but improved with increasing bias, which was attributed to anisotropy in impact ionization and asymmetric bevel angles (the latter caused by process variation and the 4° miscut of the substrate). Li et al. [5] showed that the direction of the spatial nonuniformity flipped when comparing pin and nip diodes, and argued that impact ionization alone was the cause.

In this paper, we examine the spatial uniformity of the response of 4H-SiC APDs operating in both linear and Geiger-modes by spatial mapping, unifying the behaviors observed in the two regimes. We also provide a cleaner view of the anisotropy through the use of pill-shaped devices, and rule out wafer-level variations like i-layer thickness and doping. Finally, initial results from full-band Monte Carlo modeling confirm that the substrate offcut angle is responsible asymmetric spikes in the gain for carriers generated at the edges of the device along the projection of [11$\underline{2}$0] onto the device plane.

Experimental Details

The basic structure used in this study was fabricated on commercially-available 6" 4H-SiC wafers with a 4°-offcut angle, in a p-illuminated, p^+pin configuration using the epitaxial layers indicated in Fig. 1. To form the device structure, we used a photoresist-reflow etching process to create a negative bevel of ~8°. Thermally-deposited and densified SiO_2 was used as a passivation layer and to isolate the bonding pads. After etching an optical window at the top of each mesa, ohmic contacts were formed along with a 300nm layer of SiO_2 which served as an anti-reflective coating. Most devices Prwere circular mesas with a 100 µm diameter at the base and ring contacts at the top and bottom, an example of which is shown in Fig. 2.

Once diced, individual devices were packaged onto TO-5 headers and capped with an open lid to allow UV transmission. These packages were then mounted to a socket on our custom measurement apparatus, shown in Fig. 3. The output of a pulsed UV LED operating at 285 nm was filtered and shaped to form a beam with a waist of ~10 µm. A moving stage with precision stepper motors was used to move the device along the focal plane. The photon flux is controlled by varying the pulse trigger frequency and a selectable neutral-density filter; a beam block can also be selected to allow in situ dark measurements. Optical power is calibrated by using a Si photodetector at high power levels, and a Cs-Te photocathode PMT for low power and single-counting modes. Custom printed circuit boards allow the system to be easily configured to measure either linear-mode current or Geiger-mode counts (the latter using a passive-quenching circuit). An external bias supply controls the operation of the APD. Photocurrent or counts are measured as a function of photon flux, bias, and position and used to generate spatial maps of responsivity and detection efficiency.

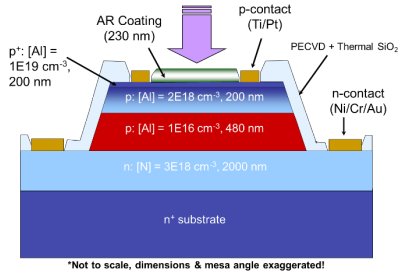

Fig. 1. Vertical structure of the avalanche photodiode.

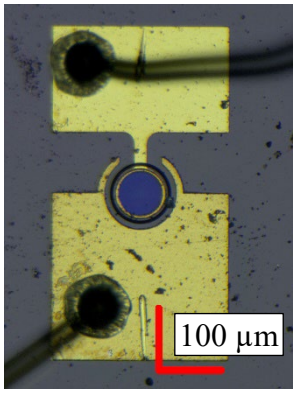

Fig. 2. Optical image of an example SiC APD.

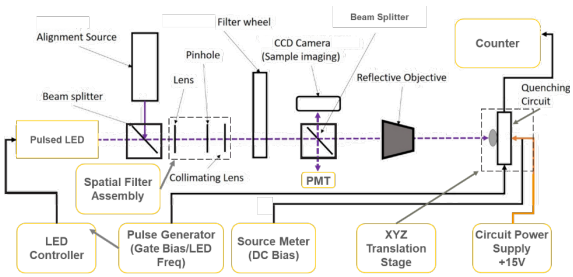

Fig. 3. Diagram of the setup used to locally illuminate a spot on the device and spatially profile photoresponse.

Fig. 4 shows a series of measured spatial maps of the responsivity (operating in linear mode) of a p-i-n SiC avalanche photodiode from unity-gain up to a dark current of 1 µA (where average gain is ~10^7). A high optical power (~50 pW) was used to ensure plenty of photosignal. The maps have all been oriented so that [11$\underline{2}$0] is parallel to the horizontal axis and [1$\underline{1}$00] is parallel to the vertical axis (i.e., if one were looking into the Si-face of the wafer, the primary wafer flat would be at the bottom). With each map, measurements of the dark current and its standard deviation are made using a beam block—the grey-shaded areas on each map are where the measured signal was noise limited. (The blue areas on the right of Figs. 4a-c are some residual current decay caused by movement of the stage as it rasters back after each line scan, and are only slightly larger than the dark current noise.)

The unity-gain responsivity in Fig. 4a equals an external quantum efficiency of 33% and is highly uniform across the optical window at the top of the mesa. The inner white ring is the location of the top ohmic contact, while the outer ring marks the edge of the mesa bevel. While uniform response is observed at unity-gain, even by Fig. 4b where the gain is less than 10^3, the responsivity is found to become increasingly non-uniform with increasing gain and characterized by localized hot-spots with values more than 10x greater than the average.

This device began to avalanche at 153.1V, corresponding to the map at 10 nA in Fig. 4e for linear mode. The series of Geiger-mode maps, shown in Fig. 5, start here as well where dark carriers start generating detectable counts. The position and orientation of the device in these maps is the same as for the linear mode maps. However, the optical power has been reduced to 100 fW and a flux of 155 k#/s. A neutral density filter with an optical density of 2.0 is used to lower the probability of coincident photons to less than 2%, ensuring single-photon counting statistics.

As expected, the two "hotspots" that formed in the upper- and lower-right sides of the linear-mode maps correspond to the exact locations where photocounts are first generated in Geiger mode, since both effects would be attributed to regions of high field. Unlike the linear-mode map, however, as the dark count rate (via more excess bias) is increased, uniformity improves since the avalanche probability cannot go above 100%. Our passive quench circuit has a "reset" time of about 5 μs, and so the dead time in the circuit begins to represent an increasing portion of the sampling time as the total count rate goes above 10-20 kHz, meaning the peak detection efficiency of 8% is likely too low.

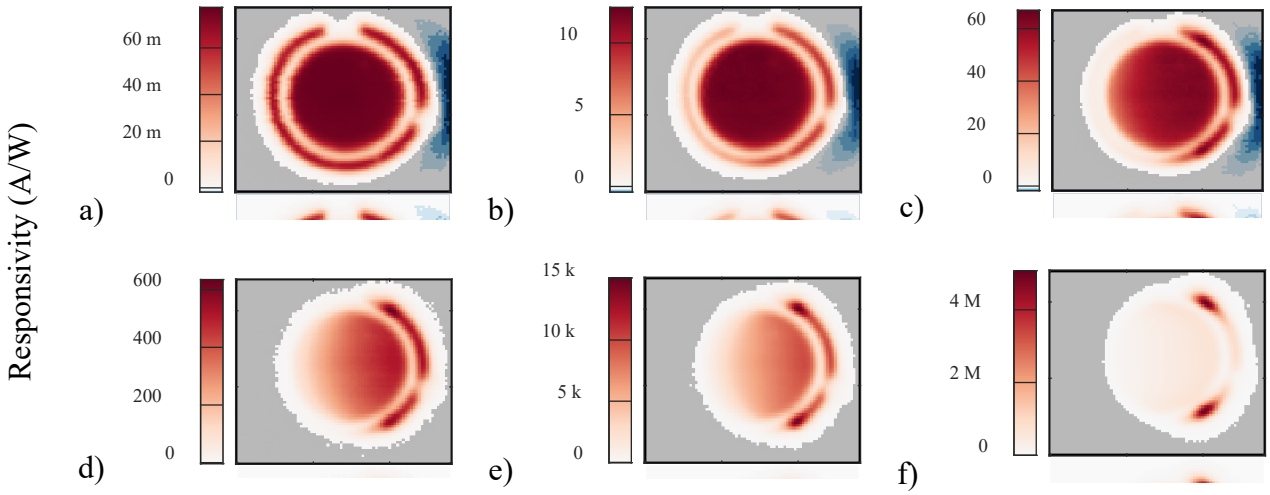

Fig. 4. Linear-mode responsivity maps for 285 nm at dark currents of a) <1 fA (unity), b) 10 pA, c) 100 pA, d) 1 nA, e) 10 nA, and f) 1 μA. The maps are oriented so that the horizontal axis is along [11$\underline{2}$0] and the vertical axis is along [1$\underline{1}$00].

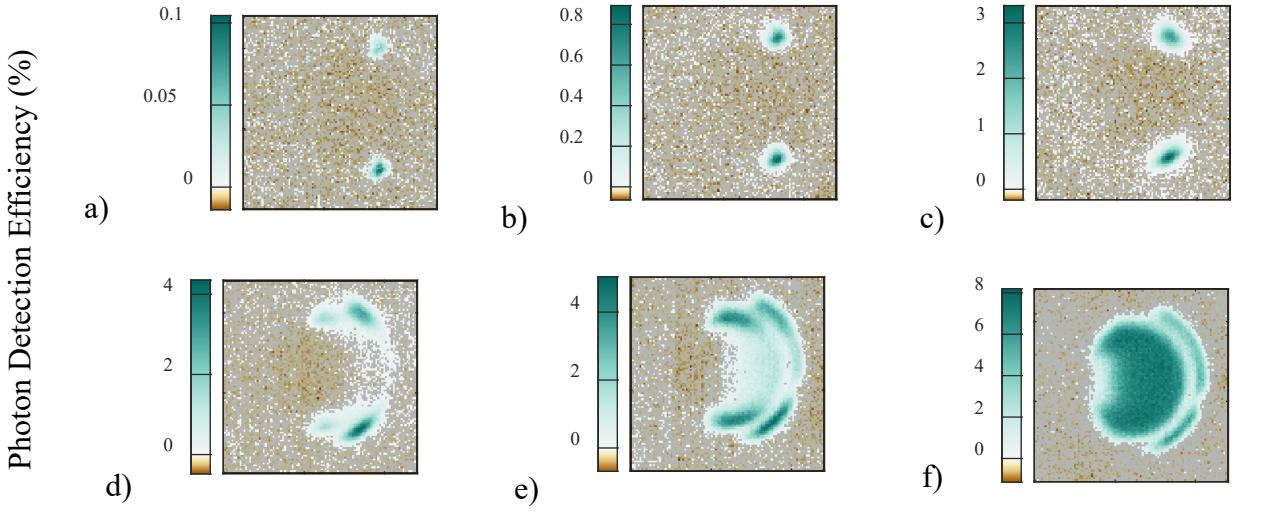

Fig. 5. Geiger-mode single-photon detection efficiency maps for 285 nm at dark-count rates of: a) 20 Hz, b) 300 Hz, c) 3 kHz, d) 10 kHz, e) 33 kHz, and f) 100 kHz. The photon flux rate was 155 kHz with a photon emission probability <2% per trigger pulse to minimize generation of coincident photons.

The spatial maps, responsivity in particular, show that there is a strong variation along [11$\underline{2}$0] but hint at uniformity in the perpendicular [1$\underline{1}$00] direction. To that end, we fabricated high aspect-ratio devices whose edges are aligned with the crystal axes, and produced devices in both parallel and perpendicular orientations. The device images and maps of linear responsivity in Fig. 6 are presented in the same orientation as our earlier data with respect to the crystal axis, although these devices are n-illuminated and therefore the direction of the spatial gradient has reversed. As before, both devices were completely uniform at unity-gain. Even when a long (>100 μm) mesa edge is perpendicular to [11$\underline{2}$0], a high degree of uniformity is maintained along [1$\underline{1}$00] with large gain. Likewise, at least to the scale of this device, the nonuniformity effect along [11$\underline{2}$0] does not appear to saturate.

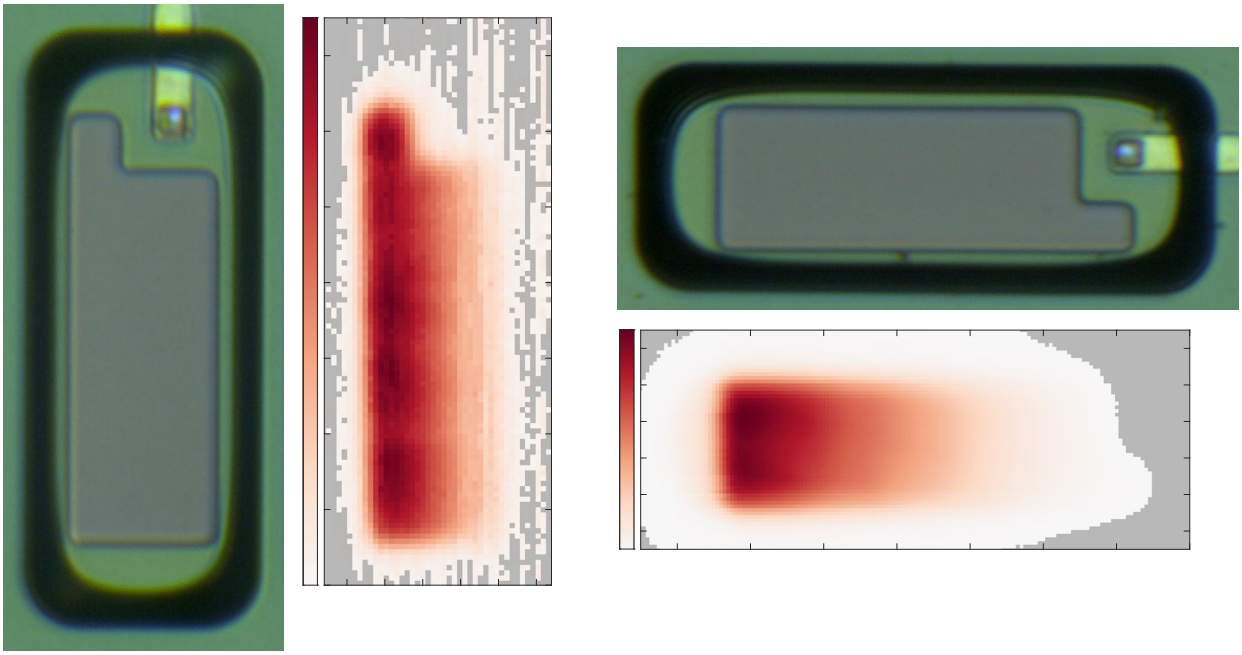

Fig. 6. Optical image (a) and responsivity map at moderate gain (b) of a "vertical" device, along with corresponding optical image (c) and responsivity map (d) of a "horizontal" device.

Numerical modeling was employed to examine the impact of two potential causes for spatial non-uniformity of the response - (1) epitaxial variation in the multiplication (drift) region of the diode, and (2) anisotropy of impact ionization and the 4° miscut of the substrate. The photocurrent in 4H-SiC APDs was calculated for varying multiplication layer thickness using Synopsys TCAD Sentaurus in which the finite element method is implemented to self-consistently solve the drift-diffusion and Poisson equations. We plot the product of the internal quantum efficiency and the gain, as this is directly proportional to the photocurrent, but more clearly shows gain is the true dependent variable, as the change in internal quantum efficiency is negligible under all the cases considered. Fig. 7 shows the expected variation in photocurrent for small changes in i-layer thickness and at various applied biases in a p-i-n APD with the n- and p- layers doped at 3 × 10^{18} and 1 × 10^{19}, respectively, and a nominal i-region thickness of 500 nm. It is evident that even at relatively low gains of <1000 (solid blue lines), minor variations in layer thickness affect

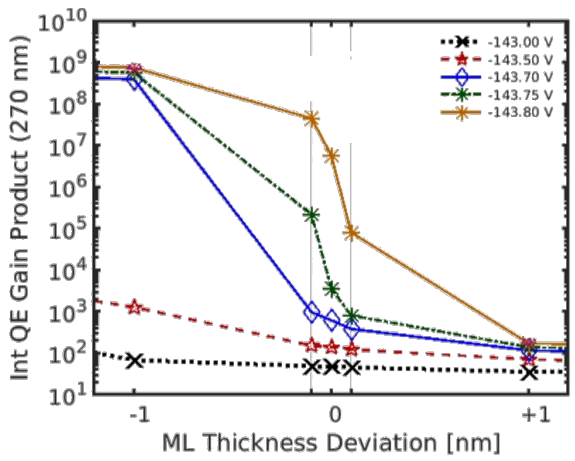

Fig. 7. TCAD simulations of QE-Gain product versus multiplication-layer thickness deviation for various biases near avalanche breakdown.

the gain by approximately half an order of magnitude, which is qualitatively similar to trends measured in real devices. Here it is important to note that a ±0.1 nm variation in i-layer thickness over the scale of a device (100 μm) is comparable to the relative variation expected across a 100 mm wafer.

However, such a thickness or doping variation due to the epitaxial growth would likely have a random or radial orientation [6] which can be detected in the nonuniformity of photoresponse. We measured the responsivity maps at moderate gain for devices in different quadrants of the same wafer—shown in Fig. 8. In each case, the nonuniformity remained aligned with the [11$\underline{2}$0] direction, suggesting that any localized variations of doping or thickness were not responsible for the phenomenon.

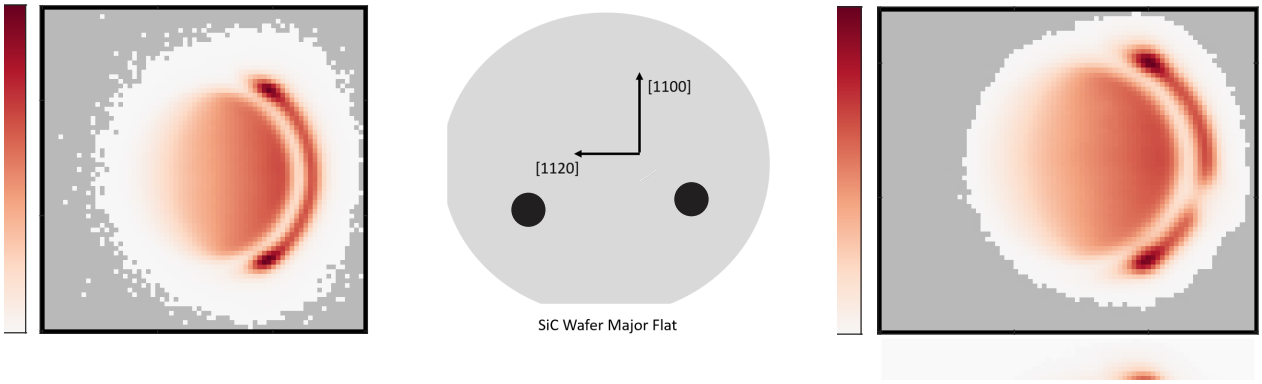

Fig. 8. Responsivity maps (a,c) and wafer location schematic (b) of two devices from different quadrants of a SiC wafer.

Finally, full-band 3D Monte Carlo calculations [7, 8] were utilized to study the influence of anisotropic impact ionization, comparing devices fabricated on-axis and with a miscut. Fig. 9 plots the calculated gain in a 4H-SiC APD that is oriented with c-axis (blue) and tilted due to a wafer miscut (red). Calculations show that while the gain in the c-axis oriented device is symmetric across the wafer, the tilted device shows strongly enhanced gain on one side and reduced gain on the opposite side. These results are attributed to the anisotropy in impact ionization in [0001] and [11$\underline{2}$0] directions and consistent with experimental data.

Summary

We performed a comprehensive study of the nonuniform gain in SiC APDs, as evidenced by changes in responsivity. Our data provides the first direct comparison of linear and Geiger mode maps, showing that the same features appear in both. By measuring devices with different orientations and at different locations on a wafer, we feel confident in concluding (as others have recently done [5]) that the impact ionization anisotropy present between [0001] and [11$\underline{2}$0] is the primary cause. Initial full-band Monte Carlo simulations match our experimental data and conclusions. At the same time, we cannot rule out influences by variations in the bevel angle when using shallow-angle bevels for suppression of the edge fields [4], which tend to be very sensitive to small changes in the angle achieved [9].

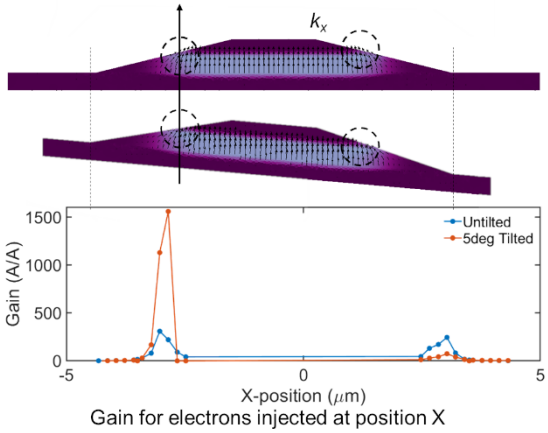

Fig. 9. Monte Carlo-simulated electric field (top) and gain versus lateral position (bottom) for tilted and untilted devices.

References

[1] X. Bai, H.D. Liu, D.C. McIntosh, J.C. Campbell, High-Detectivity and High-Single-Photon-Detection-Efficiency 4H-SiC Avalanche Photodiodes, IEEE Journal of Quantum Electronics, 45 (2009) 300-303, https://doi.org/10.1109/JQE.2009.2013093.

[2] X. Zhou, T. Han, Y. Lv, J. Li, W. Lu, Y. Wang*, et al.*, Large-Area 4H-SiC Ultraviolet Avalanche Photodiodes Based on Variable-Temperature Reflow Technique, IEEE Electron Device Letters, 39 (2018) 1724-1727, https://doi.org/10.1109/LED.2018.2871798.

[3] X. Guo, A.L. Beck, X. Li, J.C. Campbell, D. Emerson, J. Sumakeris, Study of reverse dark current in 4H-SiC avalanche photodiodes, IEEE Journal of Quantum Electronics, 41 (2005) 562-567, https://doi.org/10.1109/JQE.2005.843616.

[4] X.L. Cai, C.F. Wu, H. Lu, Y.F. Chen, D. Zhou, F. Liu*, et al.*, Single Photon Counting Spatial Uniformity of 4H-SiC APD Characterized by SNOM-Based Mapping System, IEEE Photonic Tech L, 29 (2017) 1603-1606, https://doi.org/10.1109/Lpt.2017.2735625.

[5] T. Li, Y. Zhou, X. Tao, W. Xu, D. Zhou, F. Ren*, et al.*, Study of Gain Spatial Nonuniformity in n-on-p and p-on-n 4H-SiC Avalanche Photodiodes, IEEE Photonic Tech L, 36 (2024) 465-468, https://doi.org/10.1109/lpt.2024.3367368.

[6] M.F. MacMillan, T. Oldham, V. Rengarajan, P. Wu, Improved Uniformity of Silicon Carbide Epitaxy Grown in a High-Volume Multi-Cassette Epitaxy Reactor, Mater. Sci. Forum, 924 (2018) 92-95, https://doi.org/10.4028/www.scientific.net/MSF.924.92.

[7] I. Prigozhin, S. Dominici, E. Bellotti, FBMC3D--A Large-Scale 3-D Monte Carlo Simulation Tool for Modern Electronic Devices, IEEE Transactions on Electron Devices, (2020) 1-9, https://doi.org/10.1109/ted.2020.3039482.

[8] M. Zhu, F. Bertazzi, M. Matsubara, E. Bellotti, Quantum mechanical model of crossing and anti-crossing points in 3D full-band Monte Carlo simulations, J. Appl. Phys., 135 (2024), https://doi.org/10.1063/5.0194536.

[9] B.J. Baliga, Fundamentals of Power Semiconductor Devices, Springer US, Boston, MA, 2008.